Gaborized MCS for Precise Code Phase Offset Estimation in Radionavigation

Luca Morichi[1], Alex Minetto[1], Fabio Dovis[1]
[1]*Dept. of Electronics and Telecommunications, Politecnico di Torino*, Turin, Italy

***Abstract*—In radar and radionavigation systems, waveform design optimization has mostly focused on Gabor bandwidth (GB), as a metric to infer code phase offset estimation accuracy. While optimization algorithms have maximized GB w.r.t. to specific design parameters and receiver bandwidth, they lack closed-form solutions for pulse shapes. Inspired by Gabor pulse theory, this paper presents a family of waveforms shaping multi-level coded spreading (MCS) coefficients with a Gaussian envelope, namely the Gaborized-MCS (G-MCS). These waveforms achieve nearly optimal GB performance, reflecting the trend of current optimization techniques to agnostically converge to such pulse shapes. Numerical analyses characterize the GB of the proposed signals across varying receiver bandwidths and compare them to optimized waveforms and legacy binary offset carrier modulations largely adopted in Global Navigation Satellite Systems.**

***Index Terms*—Waveform design, Gabor bandwidth, pulse shaping, optimization algorithms, Global Navigation Satellite Systems (GNSS).**

I. Introduction

In radar and radionavigation systems based on ranging codes, accurate code phase offset estimation enables the measurement of a signal's Time-Of-Arrival (TOA) and time difference of arrival (TDOA), which are crucial for determining target's location or receiver's position and local clock offset, referred hereafter as receiver state. To achieve this, signal design should be tailored to minimize the estimation uncertainty of such observables.

Alongside the use of properly-designed ranging code sequences [1], optimizing their chip shaping is equally important to enhance overall signal tracking performance [2], [3].

Traditionally, radionavigation systems, such as Global Navigation Satellite System (GNSS)s, have relied on rectangular chip shaping, applied to Binary Phase Shift Keying (BPSK) modulation and, more recently, on subcarrier modulations known as binary offset carrier (BOC). As highlighted in [4], these modulations can be regarded as special cases of multi-level coded symbol (MCS). To ensure theoretical generality, this work specifically addresses MCS modulations, particularly those with rectangular subchip shaping.

A method for optimizing chip shaping in MCS modulations with rectangular subchips has been proposed in the literature [5], [6]. This approach minimizes the Cramér-Rao lower bound (CRLB) for code phase offset estimation, representing the theoretical lower bound on unbiased estimation error in high carrier-to-noise power density ratio conditions, or *main-lobe dominated regimes* [7]. The method exploits the inverse quadratic relationship between the CRLB and the Gabor bandwidth (GB), formulating an optimization problem that seeks to maximize the latter. However, this numerical approach does not yield a closed-form expression for the optimal pulse shape. This limits the control on signal design and may lead to degenerate, unsuitable shaping waveforms.

Inspired by Gabor pulse theory [8], this study introduces a novel family of waveforms named Gaborized-MCS (G-MCS). These waveforms leverage a parametrized Gaussian envelope inherent in Gabor pulses to determine the amplitudes of the rectangular subchips shaping each chip of the ranging code.

The resulting waveforms achieve nearly optimal GB performance, supporting the notion that current optimization techniques inherently converge toward similar waveforms.

The paper is structured as follows: Section II covers baseband signal definition, CRLB, GB, and MCS modulations. Section III details G-MCS construction and key parameters. Section IV compares GB performance with optimized MCS. SectionV summarizes findings and future directions.

II. Background

In the following, modernized GNSS is assumed as valuable case study of radionavigation systems relying on spread spectrum signals. The baseband signal, as processed by the receiver, can be modeled as

$$r(t) = \sqrt{2P_R} \sum_n c_n \, x(t + nT_c - \tau) + \omega(t) \qquad (1)$$

where P_R denotes the received signal power, $\{c_n\}_{n=1}^{N}$ represents the Pseudo Random Noise (PRN) ranging codes [4], which are deterministic binary sequences ($c_n = \pm 1$) with autocorrelation properties similar to random sequences [9] and known to both the transmitter and receiver. The function $x(t)$ is the chip waveform, T_c is the chip duration, and τ represents the code phase offset between incoming signal and locally-generated replicas, measured in the receiver's time reference frame. Finally, $\omega(t)$ accounts for additive Gaussian noise, with a constant power spectral density over the receiver bandwidth of $N_0/2$ W/Hz.

In GNSS positioning, the receiver aims to estimate the code phase offset, τ, as it is essential for constructing ToA observables, which in turn are required to the receiver state estimation. Assuming that the receiver's algorithm implements an unbiased estimator, the final estimation accuracy is fundamentally constrained by the CRLB, which provides a theoretical lower limit on the variance of the estimation error

for any unbiased estimator. In the specific case of code phase offset estimation, the variance of the estimation error satisfies

$$\sigma_\tau \geq \frac{1}{8\pi^2 \frac{C}{N_0} T \beta^2} \tag{2}$$

where β is namely the signal root-mean-squared (RMS) bandwidth, also referred to as the GB, and is defined by

$$\beta = \sqrt{\frac{\int_{-\infty}^{+\infty} f^2 |X(f)|^2 df}{\int_{-\infty}^{+\infty} |X(f)|^2 df}} \tag{3}$$

where $X(f)$ is the Fourier transform of the considered time chip waveform [10]. From (2) and (3), it follows that the CRLB directly depends on the choice of chip waveforms $x(t)$. This dependency can be exploited in signal design to optimize signal properties, using the CRLB as a performance metric. In particular, the relationship between (3) and (2) suggests that designing waveforms to maximize the GB leads to a lower variance in the code phase offset estimates [11].

The GB in (3) emphasizes higher-frequency components by weighting the signal Power Spectral Density (PSD) with the square of the frequency. As a result, signals characterized by a PSD concentrated near the band edges achieve a lower CRLB.

Additionally, the GB provides insight into the shape of the correlation peak in the code phase offset domain of the Woodward ambiguity function, also known as the Cross-Ambiguity Function (CAF) [12]. A denser PSD near the channel boundaries results in a sharper correlation peak, improving resolution in code phase offset estimation.

A. Multilevel Subcarrier Modulations

Historically, BPSK was the first modulation adopted in satellite navigation systems, characterized by a rectangular waveform $x(t)$. This waveform is generally denoted as BPSK(n), where n indicates that the signal has a chip rate of $n \times f_0$, with $f_0 = 1.023$ Mcps being the reference chip rate of the GPS C/A signal.

Over time, modern GNSS signals have adopted more advanced modulation schemes, including BOC and its variants. A BOC waveform is typically denoted as BOC(m, n), where m and n are defined as $m = R_{sc}/f_0$ and $n = R_c/f_0$, respectively, whereas R_{sc} represents the subcarrier frequency and R_c the chip rate of the ranging code. The ratio $\xi = m/n$ determines the number of subcarrier cycles per code chip. Depending on whether the subcarrier is defined as $\text{sign}(\sin(2\pi f_{sc} t))$ or $\text{sign}(\cos(2\pi f_{sc} t))$, the BOC waveform is classified as sine-BOC or cosine-BOC, respectively. For brevity, we will refer to sine-BOC as $\text{BOC}_S(m, n)$ and cosine-BOC as $\text{BOC}_C(m, n)$ from now on.

Both BPSK and BOC can be interpreted as special cases of the more general class of MCS signals [4]. In an MCS signal, each chip of the spreading code is divided into K subchips of equal duration, each characterized by a specific amplitude s_k and waveform shape $w_k(t)$. More formally, the transmitted waveform can be expressed as

$$x(t) = \sum_{k=1}^{K} s_k \, w_k(t - kT_{sub}) \tag{4}$$

where s_k represents the amplitude of the k-th subchip, $w_k(t)$ defines the waveform shape of each subchip, K is the number of subchips per chip, and $T_{sub} = T_c/K$ denotes the subchip duration, with T_c being the chip duration.

From (4), it can be observed that BPSK represents the special case where $K = 1$, meaning that each chip consists of a single subchip with unit amplitude ($s_1 = 1$) and a rectangular waveform $w_1(t)$. Similarly, BOC modulation can also be expressed using (4). For instance, the $\text{BOC}_S(1, 1)$ modulation corresponds to the case where $K = 2$, meaning that each chip is divided into two subchips with alternating amplitudes ($s_1 = +1$, $s_2 = -1$), while still using a rectangular waveform.

An MCS modulation, is denoted as $\text{MCS}(\mathbf{s}, R_c)$, where $\mathbf{s} = [s_1, s_2, \ldots, s_K]$ is the amplitude vector, which consists of the amplitudes of the K subchips within a chip. The generalized PSD for such modulation schemes is defined through (5) [4].

B. MCS optimization

Within the MCS framework, [5], [6] developed a mathematical method to determine the optimal chip waveform $x(t)$ that maximizes the GB. For this purpose, they formulated the following optimization problem:

$$\begin{cases} \arg\max\limits_{\mathbf{s}} \dfrac{\int_{-\frac{\beta_r}{2}}^{\frac{\beta_r}{2}} f^2 |X(f)|^2 df}{\int_{-\frac{\beta_r}{2}}^{\frac{\beta_r}{2}} |X(f)|^2 df} \\ \text{s.t.} \quad \|\mathbf{s}\| = 1 \end{cases} \tag{6}$$

where β_r denotes the front-end bandwidth of the receiver. In [5], the authors specifically considered a rectangular subchip shape $w(t)$ and, for a given K, derived the optimal amplitudes that maximize the GB. The resulting solution ensures that no other MCS signal with same number of subchips can attain a greater GB under the given receiver front-end bandwidth constraint.

C. Gabor pulses

Gabor functions, also referred to as Gabor waveforms, pulses, or wavelets, offer several advantages in the context of code phase and frequency offset estimation, particularly in radar and sonar applications. The Gabor pulse shows unique sharpening and confining properties of the CAF correlation main lobe, which in turn reduces the uncertainty in simultaneous code phase and frequency offset estimation. The continuous-time complex definition of the Gabor pulse is reported in [13], as

$$g(t) = e^{\frac{-(t-t_0)^2}{(2\sigma_t^2)}} e^{j2\pi f_{sc}(t-t_0)} \tag{7}$$

where t is the time variable, t_0 is the center of the Gaussian envelope along the time axis, σ_t is the Gaussian Root-Mean-Square (RMS) width, and f_{sc} is the fundamental frequency of the modulating sinusoidal carrier signal.

$$G_{MCS(\mathbf{s},R_c)} = R_c \frac{\sin^2\left(\frac{\pi f}{KR_c}\right)}{(\pi f)^2} \left\{ 2\sum_{\ell=1}^{K}\sum_{m=1}^{K} s_\ell s_m \cos\left[(m-\ell)\frac{2\pi f}{KR_c}\right] - \sum_{\ell=1}^{K} s_\ell^2 \right\} \tag{5}$$

In the continuous-time domain, the minimal area of the time-frequency representation of a Gabor pulse is dictated by the uncertainty principle. This principle states that there is an inherent trade-off between the time and frequency resolutions of a signal. A more localized signal in time will result in a broader frequency bandwidth, and vice versa. The Gabor pulse effectively strikes a balance between these two properties, achieving a high degree of both time and frequency localization.

According to [14]–[16], a discrete-time, discrete-amplitude Gabor pulse does not necessarily preserve the aforementioned properties of the CAF correlation main lobe as its continuous-time, continuous-valued counterpart. The discrete pulse is described by a finite number of time and amplitude values, which limits its ability to perfectly replicate the behavior of the continuous pulse [16]. Although this level of suboptimality exists, we assume that the discrete definition still approximates its continuous-time counterpart, especially in the context of numerical signals. In this regard, we propose using a discrete Gabor function to shape the chips of the spreading code.

III. Methodology

A. Gaborized Multilevel Subcarrier Modulation

By leveraging (7), the generation of a discrete Gabor pulse involves two main parameters: the number of subchips K, and their corresponding amplitude $\mathbf{s}$ which are determined by the Gaussian envelope's RMS width described by σ_t.

We leverage the generation of a sinusoidal subcarrier, which forms the basis of BOC modulation. This subcarrier is then modulated by the amplitude of a Gaussian envelope evaluated at specific time instants.

- The chip duration is fixed as $T_c = \frac{1}{R_c}$, where R_c represents the chip rate (e.g., $R_c = 1.023$ Mcps for the nominal GPS L1 C/A code).
- The number of subchips K determines the subcarrier used in the Gabor pulse. Specifically, K is related to the BOC parameter by: $K = 2\xi = 2(m/n)$. For instance, to construct a G-MCS with eight subchips, the sinusoidal sine subcarrier used in a BOC$_s(4,1)$ modulation is employed for the quadrature component, while the cosine subcarrier is used for the in-phase component.
- To extract the K amplitude values associated with the subchips, we analyze the continuous-time Gabor pulse and identify the time instants at the nulls of the derivative of the sinusoidal subcarrier. The amplitudes of the subchips are then determined by evaluating the Gabor pulse at these time markers.

A sample in-phase and quadrature continuous-time Gabor pulse, along with its corresponding unit-norm G-MCS chip, is presented in Fig. 1. This G-MCS chip is obtained through the continuous-time Gaborization of a fundamental BOC$(4,1)$ scheme, where the Gaussian envelope RMS width is set to $\sigma_t = T_c/4$. The circular markers in Fig. 1a and Fig. 1b indicate the amplitudes of the individual subchips.

We refer to the proposed Gaborized modulation schemes as G-MCS(σ_t, m, n) in the following discussion.

B. Comparative analysis

A comparative analysis is performed by evaluating the Gabor bandwidth for G-MCS modulations and comparing it with the generating BOC and optimized MCS [6]. The signal PSD, essential for computing the GB through (3), is obtained using the analytical formulation presented in (5).

IV. Results

Fig. 3 presents four heatmaps comparing the gain (in dB-MHz) in terms of GB between four G-MCS modulations and their corresponding BOC modulations in Fig. 3a and Fig. 3c, as well as against the upper bound imposed by MCS modulations for a given number of subchips, as proposed in [6], in Fig. 3b and 3d. The G-MCS modulations under analysis are G-MCS$(\sigma_t, 3.5, 1)$ (7 subchips), G-MCS$(\sigma_t, 4, 1)$ (8 subchips), G-MCS$(\sigma_t, 6, 1)$ (12 subchips), and G-MCS$(\sigma_t, 6.5, 1)$ (13 subchips).

Fig. 3a and Fig. 3b show heatmaps for an even number of subchips, while Fig. 3c and Fig. 3d correspond to an odd number of subchips.

Each heatmap consists of four column blocks, where each block represents a specific double-sided front-end bandwidth: 10 MHz, 20 MHz, 40 MHz, and 60 MHz. Each block contains four columns, each corresponding to a specific m, n pair and the selected subcarrier (either sine or cosine).

The first row of each heatmap is separated from the others, as it contains the reference GB value (in MHz) for the given front-end bandwidth, corresponding to either the respective BOC modulation or the MCS modulation with the same number of subchips. The remaining rows of the heatmap display various G-MCS modulations with different values of σ_t for the Gaussian envelope.

The heatmaps use a grayscale color scheme: darker gray indicates a loss, medium gray represents a gain, and lighter gray denotes comparable performance. The numbers in bold represent the maximum gain for each column.

In the first place, it can be noted that there is an improvement over the BOC modulation in almost all scenarios. When σ_t approaches T_c, the "filtering" contribution of the Gaussian envelope is minimal, which is why the modulations in the first two rows of the heatmap in Fig. 3a and Fig. 3c have values equal to zero. The most significant losses across all

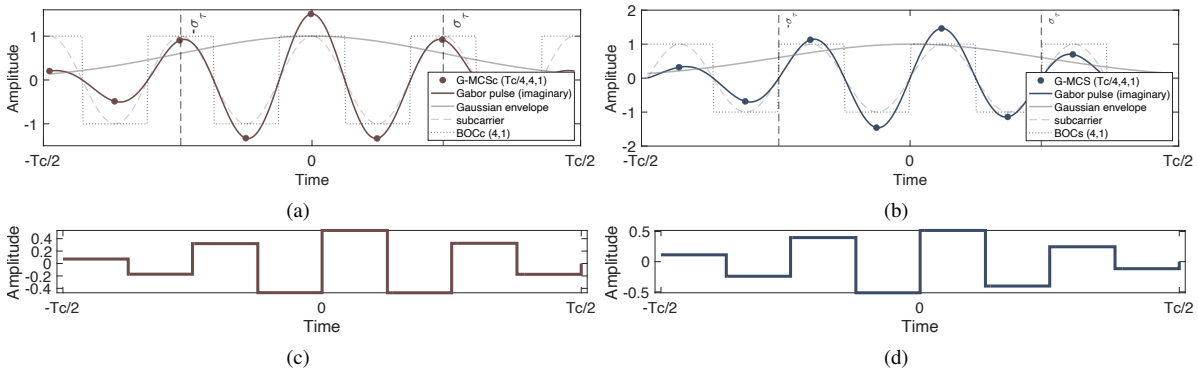

Fig. 1: Continuous-time (upper) to discrete-time (lower) view of in-phase and quadrature components of a sample G-MCS, i.e., G-MCS$(Tc/4, 4, 1)$ with $Tc = 1/(1.023 \times 10^6)$.

heatmaps occur for the $m = 6$ and $n = 1$ pair in the 10 MHz front-end bandwidth. However, this is explainable since this bandwidth does not encompass the two PSD main lobes, which are centered at ± 6 MHz, respectively (refer to Fig. 2). Fig. 2 shows the PSDs for the cosine G-MCS modulations under analysis. The effect of the main lobe positions can be observed, which follow the applied subcarrier. Regarding the comparison with the best MCS, it can be observed that the upper bound is not exceeded, but a very close approach is achieved with nearly every G-MCS configuration, and in some cases, identical performance is reached (at least up to the second decimal place). Among all the configurations, the ones with $\sigma_t = T_c/3$ and $\sigma_t = T_c/4$ show the best performance. Fig. 4 shows the behavior of the GB as the front-end bandwidth increases up to 60 MHz for the four G-MCS modulations under test with $\sigma_t = T_c/3$. These configurations exhibit nearly optimal performance across all bandwidths, with slightly lower values compared to the upper bound defined by the optimized MCS from [6]. From both Fig. 3 and Fig. 4, it can be observed that, regardless of whether the G-MCS modulation is in phase or in quadrature, the resulting GB performance is essentially the same. Additionally, for bandwidths greater than 11.5 MHz, all G-MCS modulations follow a trend fully consistent with BOC modulations, but with a consistent improvement in GB values. The comparison with the optimized MCS further demonstrates the near-optimal GB performance of the proposed G-MCS modulations.

V. Conclusion

This work explores the use of discrete Gabor pulses to define G-MCS subcarrier modulation for radionavigation signals, referred to as G-MCS. The proposed modulation shows no degradation of performance w.r.t. to legacy BOC modulations employed in GNSS. More importantly, it achieves near-optimal performance when compared to the upper bound defined in [6], by disclosing a closed form suitable to numerical signal generation. This preliminary study lays the groundwork for characterizing G-MCS based on further key performance metrics, including out-of-band unwanted emissions, spectral separation coefficient, multipath and interference error envelopes, and correlation loss in presence of signal distortions.

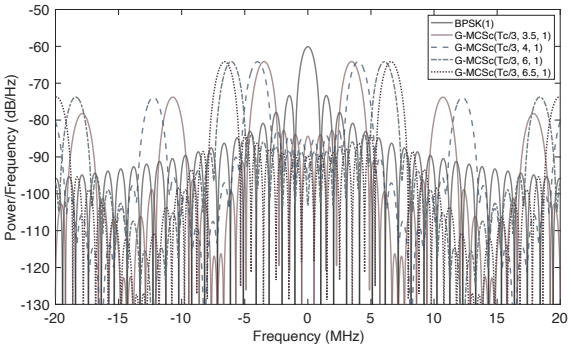

Fig. 2: PSD of G-MCS(Tc/3, m, n) with $n = 1$ and $m \in \{3.5, 4, 6, 6.5\}$, and BPSK(1).

Acknowledgment

Funded by the European Union - NextGenerationEU, Mission 4 Component 2 - ECS00000036 - CUP E13B22000020001

References

[1] S. W. Golomb and G. Gong, *Signal design for good correlation: for wireless communication, cryptography, and radar*. Cambridge University Press, 2005.

[2] L. Giugno and M. Luise, "Optimum pulse shaping for delay estimation in satellite positioning," in *2005 13th European Signal Processing Conference*. IEEE, 2005, pp. 1–6.

[3] J. A. Nossek and F. Antreich, "On chip pulse shape design for precise synchronization of DS-CDMA systems," *International Journal of Circuit Theory and Applications*, vol. 35, no. 5-6, pp. 565–574, 2007.

[4] J. Á. Ávila Rodríguez, "On generalized signal waveforms for satellite navigation," PhD thesis, München, Univ. der Bundeswehr, June 2008.

[5] X. Zhang, Z. Yao, and M. Lu, "Optimizing the Gabor bandwidth of satellite navigation signals by MCS signal expression," *Science China Physics, Mechanics and Astronomy*, vol. 54, pp. 1077–1082, 2011.

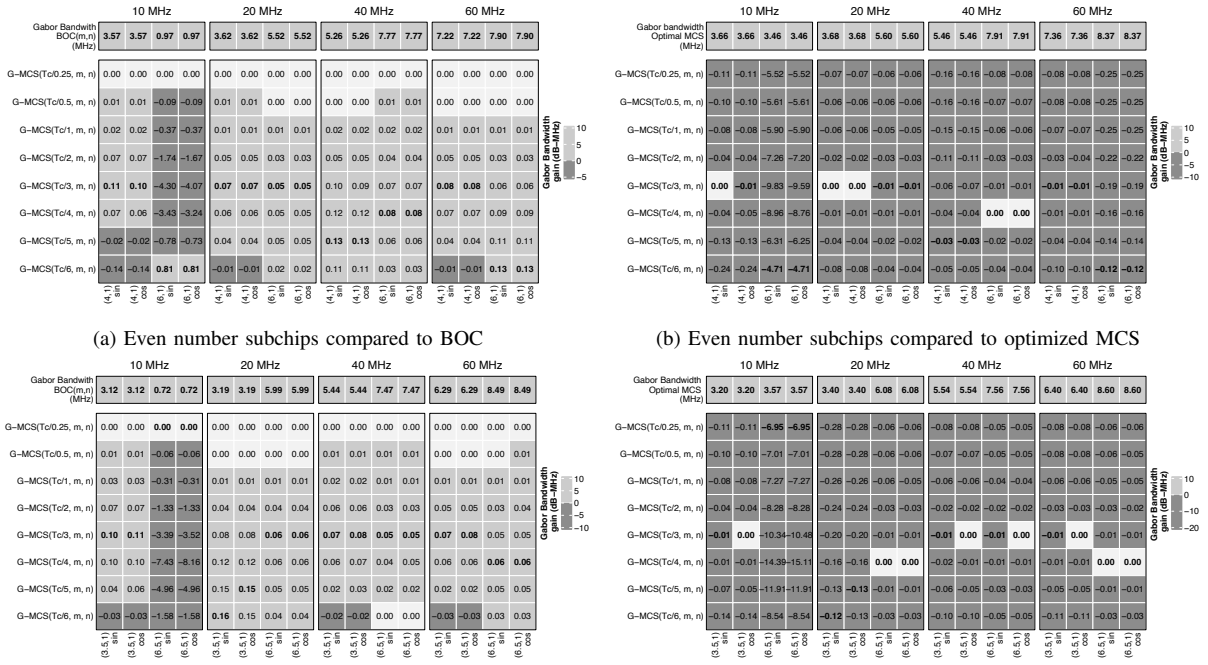

(a) Even number subchips compared to BOC

(b) Even number subchips compared to optimized MCS

(c) Odd number subchips compared to BOC

(d) Odd number subchips compared to optimized MCS

Fig. 3: Gain in terms of GB for G-MCS modulations with both even and odd numbers of subchips, compared to BOC and optimized MCS.

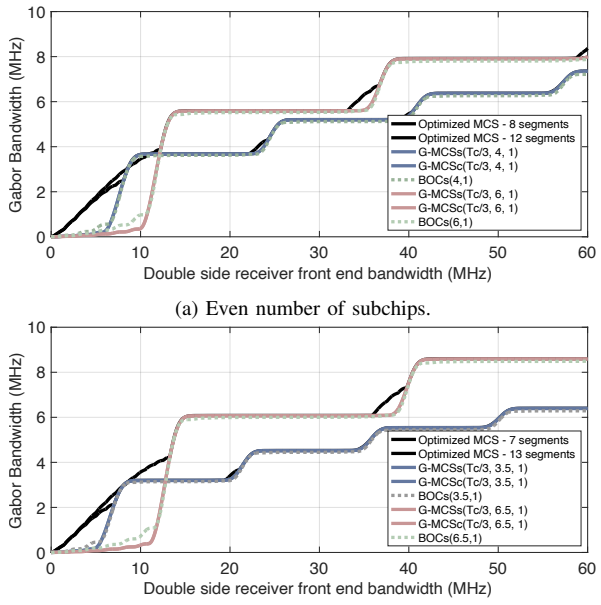

(a) Even number of subchips.

(b) Odd number of subchips.

Fig. 4: GB comparison between G-MCS, BOC, and the optimized MCS [6].

[6] X. Zhang, Z. Yao, X. Zhang, and M. Lu, "A method to optimize the spreading code chip waveform in sense of Gabor bandwidth," in *Proceedings of the 24th international technical meeting of the satellite division of the institute of navigation (ION GNSS 2011)*, 2011, pp. 1299–1304.

[7] J. Ziv and M. Zakai, "Some lower bounds on signal parameter estimation," *IEEE transactions on Information Theory*, vol. 15, no. 3, pp. 386–391, 1969.

[8] R. Parhizkar, Y. Barbotin, and M. Vetterli, "Sequences with minimal time–frequency uncertainty," *Applied and Computational Harmonic Analysis*, vol. 38, no. 3, pp. 452–468, 2015. [Online]. Available: https://www.sciencedirect.com/science/article/pii/S1063520314000906

[9] H.-J. Zepernick and A. Finger, *Pseudo random signal processing: theory and application*. John Wiley & Sons, 2013.

[10] S. M. Kay, "Fundamentals of statistical signal processing: Estimation theory," 1993.

[11] J. W. Betz and K. R. Kolodziejski, "Generalized theory of code tracking with an early-late discriminator part i: Lower bound and coherent processing," *IEEE Transactions on Aerospace and Electronic Systems*, vol. 45, no. 4, pp. 1538–1556, 2009.

[12] P. M. Woodward, "Radar ambiguity analysis," Royal Radar Establishment, Malvern, UK, Tech. Rep. RRE-TN-731, 1967.

[13] S. Qian and D. Chen, "Discrete Gabor transform," *IEEE transactions on signal processing*, vol. 41, no. 7, pp. 2429–2438, 2002.

[14] R. A. Haddad, A. N. Akansu, and A. Benyassine, "Time-frequency localization in transforms, subbands, and wavelets: a critical review," *Optical Engineering*, vol. 32, no. 7, pp. 1411–1429, 1993.

[15] J. Ramanathan and P. Topiwala, "Time–frequency localization and the spectrogram," *Applied and Computational Harmonic Analysis*, vol. 1, no. 2, pp. 209–215, 1994.

[16] R. Parhizkar, Y. Barbotin, and M. Vetterli, "Sequences with minimal time–frequency uncertainty," *Applied and computational harmonic analysis*, vol. 38, no. 3, pp. 452–468, 2015.